Theorem 2: The system (1) optimized with respect to the performance index (8) remains stable even after the optimal control law $u^* = -\frac{1}{2}G^T\nabla n(x)$ is changed to either

$$\text{(i)} \quad u^* = -\tfrac{1}{4}G^T\nabla n(x) - \psi \tag{29}$$

where ψ is a nonlinear vector function of $\frac{1}{2}G^T\nabla n(x)$, satisfying $\sigma^T\psi(\sigma) > 0$ with

$$\sigma = \tfrac{1}{2}G^T\nabla n(x), \quad \sigma \neq 0 \tag{29a}$$

or

$$\text{(ii)} \quad u = -\tfrac{1}{2}k(t)G^T\nabla n(x) \tag{30}$$

with, for all t,

$$\tfrac{1}{2} + \epsilon \leq k(t) \leq \bar{k} < \infty \tag{31}$$

with $\bar{k}$ arbitrary.

Proof: (i) The closed loop system after the introduction of nonlinearity in the optimal control is

$$\dot{x} = Fx - \tfrac{1}{4}GG^T\nabla n(x) - G\psi \tag{32}$$

Using as the Lyapunov function $V = n(x)$

$$\dot{V} = \nabla^T n(x)[Fx - \tfrac{1}{4}GG^T\nabla n(x) - G\psi] = x^TF^T\nabla n(x) - \tfrac{1}{4}\nabla^T n(x)GG^T\nabla n(x) - G\psi = -k!m_k(x) - G^T\nabla n(x)\psi$$

the last line following by use of the Hamilton-Jacobi Eq. (28). Evidently $\dot{V}$ is always nonpositive establishing stability.

(ii) Proof in the case when time variation is introduced into the optimal control law follows easily. It can be seen that Theorem 2 is valid even when the system is nonlinear, i.e., $\dot{x} = F(x,u)$ where $F(x,u)$ is a nonlinear function of x and u, provided an optimal control exists which makes the closed loop system asymptotically stable.

Appendix

Proof of the lemma

Consider $(d/dt)[t^l m_{j+1}(x)]$ for $l,j = 0,1,\ldots,k$ along the trajectories of Eq. (9).

$$(d/dt)[t^l m_{j+1}(x)] = lt^{l-1}m_{j+1}(x) + t^l(d/dt)m_{j+1}(x) = lt^{l-1}m_{j+1}(x) - t^l m_j(x) \tag{A1}$$

assuming

$$(d/dt)[m_{j+1}(x)] = -m_j(x), \quad j = 0,1,\ldots,k \tag{A2}$$

Since the system (9) is asymptotically stable, (A2) gives a positive definite $m_{j+1}(x)$ for positive definite $m_j(x)$. From Eq. (A1)

$$\int_0^\infty t^l m_j(x)dt = \int_0^\infty lt^{l-1}m_{j+1}(x)dt - t^l m_{j+1}(x)\Big|_{t=0}^{\infty} = \int_0^\infty lt^{l-1}m_{j+1}(x)dt$$

since Eq. (9) is asymptotically stable. Therefore

$$\begin{aligned}\int_0^\infty t^k m_0(x)dt &= \int_0^\infty kt^{k-1}m_1(x)dt \\ &= \int_0^\infty k(k-1)t^{k-2}m_2(x)dt \\ &\;\;\vdots \\ &= \int_0^\infty k!m_k(x)dt \\ &= -\int_0^\infty k!\frac{d}{dt}m_{k+1}(x)dt \\ &= k!m_{k+1}(x_0)\end{aligned} \tag{A3}$$

where

$$(d/dt)m_{j+1}(x) = -m_j(x), j = 0,1,\ldots,k \tag{A4}$$

along the trajectories of Eq. (9).

References

[1] Anderson, B. D. O. and Moore, J. B., "Tolerance of Nonlinearities in Time-Varying Optimal Systems," *Electronics Letters*, Vol. 3, No. 6, June 1967.

[2] Anderson, B. D. O., "Stability Results for Optimal Systems," Electronics Letters, Vol. 5, No. 22, Oct. 1969, p. 545.

[3] MacFarlane, A. G. J., "The Calculation of Functionals of Time and Frequency Responses of a Linear Constant Coefficient Dynamical System," *Quarterly Journal of Mechanics and Applied Mathematics*, Vol. 16, Pt. 2, 1963, pp. 259–271.

[4] Man, F. T. and Smith, H. W., "Design of Linear Regulators Optimal for Time-Multiplied Performance Indices," *IEEE Transactions on Automatic Control*, Vol. AC-14, Oct. 1969, pp. 527–529.

Transient Behavior of Charring Ablators

JAY R. ROLAND* AND MARTIN C. JISCHKE†

University of Oklahoma, Norman, Okla.

INTEREST in thermal protection devices for very high-speed re-entry has led to the study of charring ablators. The behavior of a phenolic nylon ablator subjected to transient heat inputs has recently been investigated experimentally.[1] These data indicate the average pyrolysis mass-loss rate to be greater under increased heating than decreased heating. It was then concluded that "there is an intrinsic difference between material behavior in increasing and in decreasing heating." This result provided the impetus for a theoretical calculation using a simplified model of the transient behavior of charring ablators.

The one-dimensional transient heat-transfer model employed is similar to that of Barriault and Yos[2] and Adarkar and Hartsook.[3] The decomposition and chemical interactions of the original ablator material (virgin) are characterized in the current model by a constant temperature decomposition, absorption of heat (heat of pyrolysis), yielding of a residue matrix (char), and evolving gaseous products (pyroly-

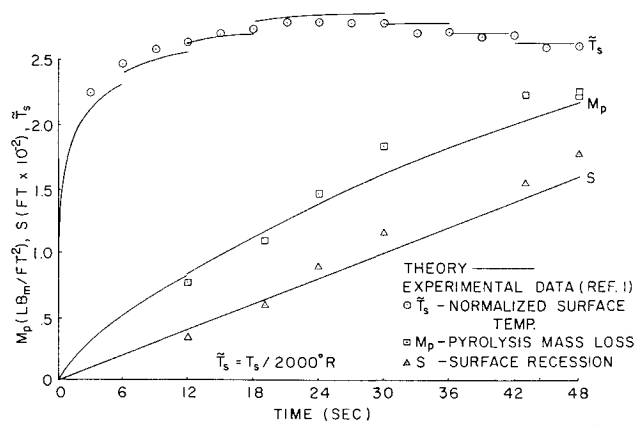

Fig. 1 Transient heating results for direct cycle.

Received February 16, 1970.

* Major, U.S. Air Force; Graduate Student, School of Aerospace and Mechanical Engineering. Member AIAA.

† Assistant Professor, School of Aerospace and Mechanical Engineering. Member AIAA.

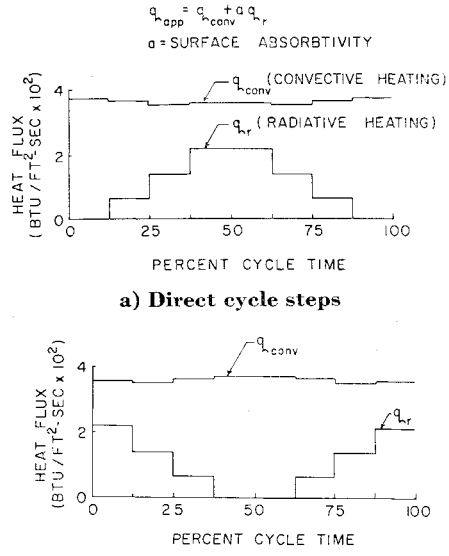

Fig. 2 Applied heating cycles.

sis gases). Whereas the detailed depolymerization, vaporization, and chemical cracking processes are not well understood, the present constant-temperature decomposition model appears to predict well the gross behavior of charring ablators. Homogeneous combustion and aerodynamic blocking are included through use of homogeneous combustion and blockage factors. With the exception of the char thermal conductivity which is taken to be an empirically determined function of temperature, all material properties are assumed constant and are determined by comparison with steady-state experimental results. The same constant material properties are employed in the transient calculations.

The theoretical calculations employ the numerical heat-balance-integral method of Goodman[4] and are similar to those of Adarkar and Hartsook.[3] For brevity, we shall omit the details of the calculational procedure and proceed directly to the results.

The calculated surface temperature T_s, surface recession S, and pyrolysis mass loss M_p along with the corresponding experimental data are shown in Fig. 1 for the so-called direct heating cycle. The direct heating cycle and an associated inverted heating cycle are shown in Fig. 2. The heats applied to the char surface over the direct and inverted heating cycles are equal. As is evident, the theoretical results compare favorably with the experimental data. The theoretical average pyrolysis mass-loss rate from step two to the midpoint of the cycle is 0.048 lbm/ft²-sec as compared to 0.035 lbm/ft²-sec from the midpoint to the end of step six. The

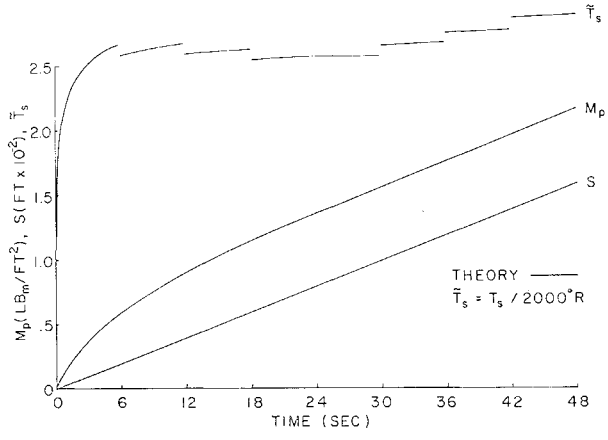

Fig. 3 Transient heating results for inverted cycle.

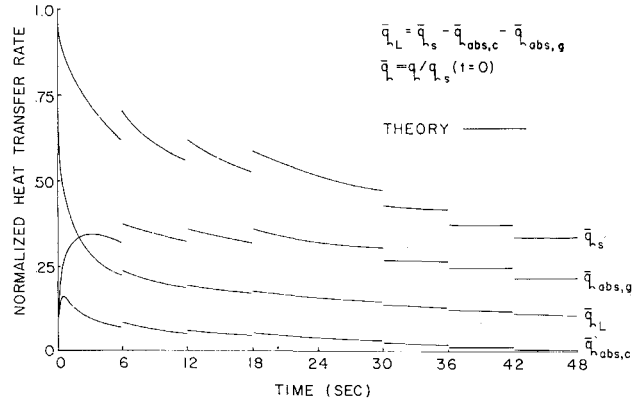

Fig. 4 Char heat balance.

corresponding experimental values are 0.057 lbm/ft²-sec and 0.041 lbm/ft²-sec, respectively. While the theoretical values are somewhat low, the lower mass-loss rate over the second half of the cycle is predicted. This is interpreted in Ref. 1 as implying an intrinsic difference in material behavior in increasing and decreasing heating.

The calculated surface temperature, surface recession, and pyrolysis mass-loss for the inverted heating cycle is shown in Fig. 3. The average mass-loss rate from step two to the midpoint of the cycle is 0.043 lbm/ft²-sec and 0.034 lbm/ft²-sec from the midpoint of the cycle to the end of step six. Thus, the average pyrolysis mass-loss rate is again higher over the first half of the cycle (decreased heating) than over the second half (increased heating). Thus, it would appear that there is no intrinsic difference between ablator behavior in increasing and decreasing heating, but that the difference is between the first and second half of the cycle.

The reason for this behavior can be seen by examining the various components of the heat flux at the boundaries of the char (Fig. 4). The heat flux leaving the back face of the char (q_L) is the heat flux available for decomposing the virgin and raising its enthalpy. As q_L is less over the second half of the cycle, the decomposition rate would be expected to, and does, follow the same trend. From Fig. 4, it is also seen that the heat flux absorbed by the char ($q_{abs,c}$) and that absorbed by the pyrolysis gases in the char ($q_{abs,g}$) are greater over the first half of the cycle; thus, this absorption does not account for q_L being less over the second half of the cycle. Clearly the results indicate the conductive heat flux entering the char surface (q_S) is less over the second half of the cycle and this accounts for q_L being less.

The various components of the heat flux entering the char surface (q_S) are shown in Fig. 5. The applied heat flux (q_{app}) is not shown as it is the same over both halves of the cycle. Calculation shows the combustion heating ($q_{comb,g}$) minus the

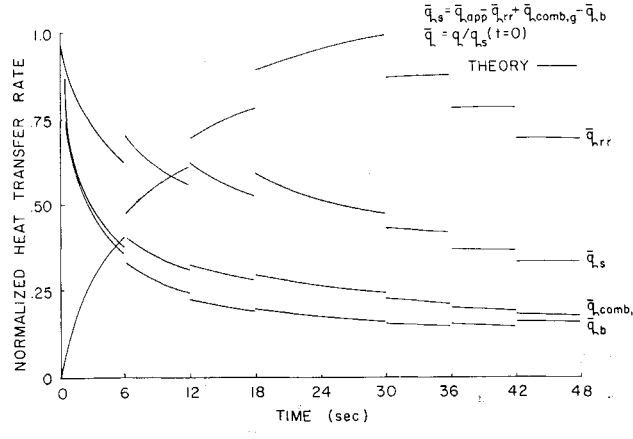

Fig. 5 Surface heat balance.

aerodynamic blockage (q_b) yields a net heat flux input which is slightly greater over the first half of the cycle, but not enough to account fully for the trend in q_L. The apparent dominant factor is the heat flux reradiated from the surface (q_{rr}) which is seen to be appreciably greater over the second half of the cycle. A similar result is obtained for the inverted heating cycle Thus, reradiation from the char surface appears to be the main reason for the average pyrolysis mass-loss rate being greater during the first half of the heating cycle. This result might be anticipated if one notes that the surface temperature is greater over the last half of the heating cycle than over the first half. This observation is true for both the theoretical and experimental results.

References

[1] Wakefield, R. M. and Lundell, J. H., "Comparison of the Performance of a Charring Ablator Under Transient and Constant Combined Convective and Radiative Heating," AIAA Paper 69-151, New York, 1969.

[2] Barriault, R. J. and Yos, J., "Analysis of the Ablation of Plastic Heat Shields that Form a Charred Surface Layer," *ARS Journal*, Vol. 30, No. 9, Sept. 1960, pp. 823–829.

[3] Adarkar, D. B. and Hartsook, L. B., "An Integral Approach to Transient Charring Ablator Problems," *AIAA Journal*, Vol. 4, No. 12, Dec. 1966, pp. 2246–2248.

[4] Goodman, T. R., "The Heat-Balance Integral and Its Application to Problems Involving a Change of Phase," *Transactions of the ASME, Ser. C: Journal of Heat Transfer*, Vol. 80, No. 2, Feb. 1958, pp. 335–342.

Response of a Low-Speed Flame to Flame-Holder Vibration

FERRIS O. GARRETT JR.* AND RAYMOND V. KASER†
University of Oklahoma, Norman, Okla.

Nomenclature

A/F = air-fuel ratio
D = flame-holder diameter
L = flame-front characteristic length
V = air-fuel mixture velocity
ϵ = density ratio across flame front
λ = wavelength
φ = Markstein parameter

Introduction

EXPERIMENTAL observations have shown that the small disturbances produced by a vibrating flame-holder may, under certain conditions, be transmitted along the flame front. This response appears on schlieren flame photographs as evenly spaced wrinkles along the flame front. This phenomenon has been the object of several analytical and experimental studies. In general, these studies have attempted to predict the regime of "flame stability." Flame stability, generally associated with lean and rich mixture flammability limits, in the present context deals with the flame response to disturbances in the flow. A stable condition exists when these disturbances decay with time and are not transmitted along the flame front.

Markstein's[1] classic work on the subject of flame stability predicts that a flame will be stable to disturbances of short wavelengths (high frequencies) and unstable to long wavelengths (low frequencies). The wavelength at which this transition occurs is known as the cutoff wavelength ($\lambda_{c.o.}$). In the development of flame stability theories, the presence of a flame-holder is not considered. The purpose of this work was to determine experimentally the effect of flame-holder diameter on cutoff wavelength, and thus flame stability, of a low-speed air-propane flame. To accomplish this, various air-fuel ratios, mixture velocities, and flame-holder sizes were used in the experiments. The range of air-fuel ratios, from 10 to 22, gave a wide spread of rich and lean mixtures. Mixture velocities of 8, 12, and 16 fps were used and flame-holder diameters were varied from $\frac{1}{8}$ in. to $\frac{3}{4}$ in. The range of Reynolds number based on flame-holder diameter and mixture speed was 600–3000.

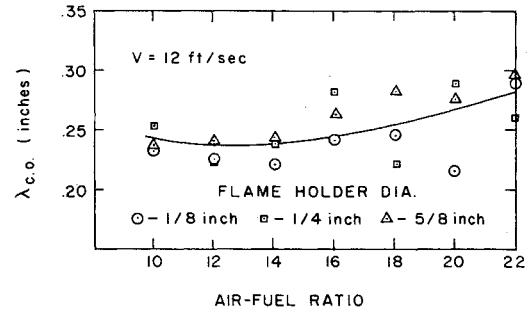

Fig. 1 Cutoff wavelength vs air-fuel ratio and flame-holder diameter.

Analysis

Analytical studies of flame stability have been carried out by applying the small perturbation technique to the governing nonlinear differential equations. Various stability theories have been developed by Landau, Markstein, Eckhaus, Einbinder, and Parlange and Chu. These theories are discussed in detail in Ref. 2. Markstein's stability theory has been verified over the lean A/F range by Petersen,[3] and the results of the present work are correlated on the basis of the Markstein theory.

This theory predicts the cutoff wavelength to be

$$\lambda_{c.o.} = 4\pi\mu L\epsilon/(\epsilon - 1) \qquad (1)$$

The density ratio ϵ can be calculated and thus a measurement of the cutoff wavelength can be used to determine μL. This quantity can also be determined from a measurement of the natural wavelength which appears on the flame front with no external excitation by making use of the Markstein maximum theory.[3]

Experimental Results

The experiments[4] were performed in the University of Oklahoma Combustion Tunnel. The flame-holder was linked

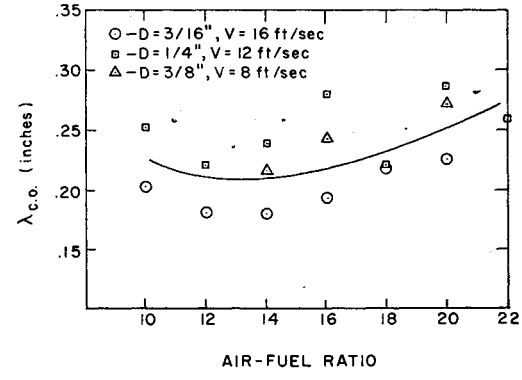

Fig. 2 Cutoff wavelength vs air-fuel ratio at constant Reynolds number (1300).

Received February 20, 1970; revision received April 29, 1970.

* Graduate Student 1968–1970; now Captain, U.S. Air Force.

† Assistant Professor, Department of Aerospace and Mechanical Engineering. Member AIAA.